

Polypeptide organic radical batteries

<https://doi.org/10.1038/s41586-021-03399-1>

Received: 13 May 2020

Accepted: 26 February 2021

Published online: 5 May 2021

 Check for updates

Tan P. Nguyen^{1,4}, Alexandra D. Easley^{2,4}, Nari Kang², Sarosh Khan¹, Soon-Mi Lim¹, Johannes H. Rezenom¹, Shaoyang Wang³, David K. Tran¹, Jingwei Fan¹, Rachel A. Letteri¹, Xun He¹, Lu Su¹, Cheng-Han Yu¹, Jodie L. Lutkenhaus^{1,3}✉ & Karen L. Wooley^{1,2,3}✉

In only a few decades, lithium-ion batteries have revolutionized technologies, enabling the proliferation of portable devices and electric vehicles¹, with substantial benefits for society. However, the rapid growth in technology has highlighted the ethical and environmental challenges of mining lithium, cobalt and other mineral ore resources, and the issues associated with the safe usage and non-hazardous disposal of batteries². Only a small fraction of lithium-ion batteries are recycled, further exacerbating global material supply of strategic elements^{3–5}. A potential alternative is to use organic-based redox-active materials^{6–8} to develop rechargeable batteries that originate from ethically sourced, sustainable materials and enable on-demand deconstruction and reconstruction. Making such batteries is challenging because the active materials must be stable during operation but degradable at end of life. Further, the degradation products should be either environmentally benign or recyclable for reconstruction into a new battery. Here we demonstrate a metal-free, polypeptide-based battery, in which viologens and nitroxide radicals are incorporated as redox-active groups along polypeptide backbones to function as anode and cathode materials, respectively. These redox-active polypeptides perform as active materials that are stable during battery operation and subsequently degrade on demand in acidic conditions to generate amino acids, other building blocks and degradation products. Such a polypeptide-based battery is a first step to addressing the need for alternative chemistries for green and sustainable batteries in a future circular economy.

Organic radical batteries promise increased environmental friendliness, independence from strategic metals and faster charging rates compared to lithium-ion batteries^{3,4,9–14}. However, a key challenge, even taking into account the beneficial aspects of organic polymer materials, is the design of functional plastics with an end-of-life consideration¹⁵. The most-studied active materials in organic radical batteries are polymers that carry redox-active pendant groups^{10,13,14,16,17}—such as 2,2,6,6-tetramethyl-4-piperidine-1-oxyl (TEMPO) and 4,4'-bipyridine derivatives (viologen)^{11,16,18–20}—along non-degradable, aliphatic backbones^{5,20–23}. Although a few studies have investigated redox-active degradable polymers and others have explored fully polymeric batteries (Extended Data Table 1)^{11,12,24–28}, none has combined these two concepts to create fully polymeric metal-free batteries that degrade on demand, which would be a first step towards the design of sustainable, recyclable batteries^{11,12,24–27}. We postulate that redox-active pendant groups along a polypeptide backbone might provide a suitable material platform for degradable organic radical batteries²⁹.

Here we report an on-demand-degradable, polypeptide-based battery (Fig. 1). We designed and synthesized polypeptide anodes and cathodes that contain redox-active pendant groups, determined their redox activities and established their behaviours in all-polypeptide batteries. First, each polypeptide was assembled into a lithium metal

half-cell battery to elucidate its fundamental energy-storage characteristics. Then, we constructed a metal-free, polypeptide-based battery. As a demonstration of recyclability, we conducted hydrolytic degradation under acidic conditions and determined the degradation products. In addition, we quantified the effects of the intact redox-active polypeptides and their degradation products on the viabilities of three different cell types. By merging degradable polypeptide backbones with the energy-storage properties of the redox-active moieties, this bioinspired polypeptide-based battery addresses some of the challenges of conventional lithium-ion batteries (for example, the use of scarce resources, safety concerns and high-cost recycling).

Syntheses of redox-active polypeptides

From L-glutamic acid as a common starting amino acid, two divergent five-step synthetic pathways were used to prepare distinct anodic and cathodic L-glutamate-based polypeptides—viologen polypeptide and biTEMPO polypeptide, respectively (Fig. 2). Both pathways began with esterification reactions to install chloro or alkynyl groups at the γ -position³⁰ (which were later used to incorporate the final redox-active moieties), followed by cyclization to establish monomer structures and then polymerization to produce poly(L-glutamates) (Fig. 2a).

¹Department of Chemistry, Texas A&M University, College Station, TX, USA. ²Department of Materials Science and Engineering, Texas A&M University, College Station, TX, USA. ³Artie McFerrin Department of Chemical Engineering, Texas A&M University, College Station, TX, USA. ⁴These authors contributed equally: Tan P. Nguyen, Alexandra D. Easley. ✉e-mail: jodie.lutkenhaus@tamu.edu; wooley@chem.tamu.edu

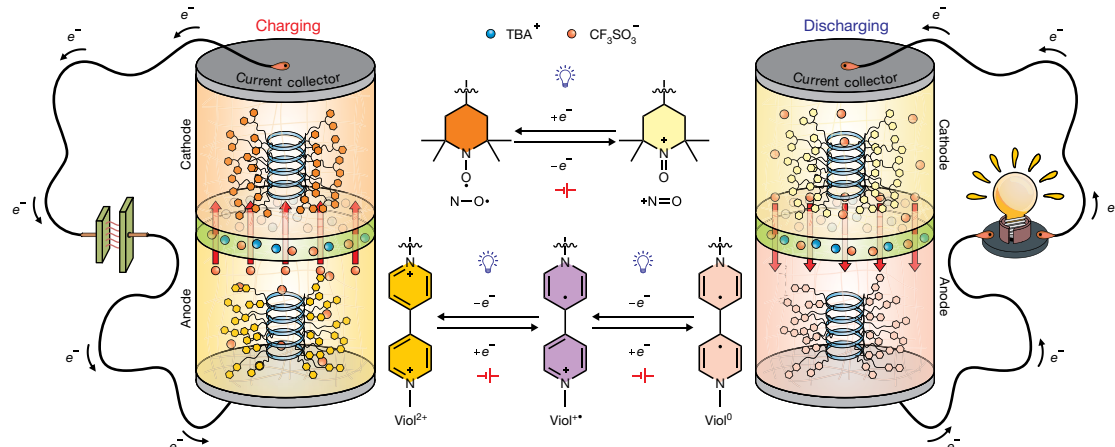


Fig. 1 | A polypeptide-based organic radical battery. Schematics of a polypeptide-based organic radical battery and the reactions that occur during charging and discharging are shown on the left and right, respectively. The redox reactions for the TEMPO (top) and viologen (bottom) pendant groups

are shown in the middle. For example, during charging, nitroxide radical functional groups at the cathode oxidize to oxoammonium cations, and viologen functional groups at the anode reduce to their neutral forms.

The synthesis of viologen polypeptide involved activation of the chloro side-chain functionality to allow for efficient installation of the dicationic oxidized form of the viologens. The synthesis of biTEMPO polypeptide involved the opposite sequence of installation of TEMPO precursors onto the alkynyl side chain, followed by activation to the nitroxide radical state (Fig. 2b).

The chloro- and alkynyl-containing polypeptides were synthesized (Fig. 2b) via ring-opening polymerization of γ -(6-chlorohexyl)-L-glutamate *N*-carboxyanhydrides (CHLG NCAs; **3**) and γ -propargyl-L-glutamate *N*-carboxyanhydrides (PLG NCAs; **11**), prepared from chloro- and propargyl-decorated L-glutamic acids, respectively, as the first two steps of the five-step sequence. The ring-opening polymerization reactions were monitored using attenuated total reflectance Fourier transform infrared spectroscopy by the decrease in intensity of the anhydride absorption of *N*-carboxyanhydrides at about 1,780 cm^{-1} . On completion, poly(γ -(6-chlorohexyl)-L-glutamate) (PCHLG; **4**) and poly(γ -propargyl-L-glutamate) (PPLG; **12**) were obtained with degrees of polymerization of about 50 (as confirmed by ^1H nuclear magnetic resonance (NMR) spectroscopy; Supplementary Figs. 14, 22) and narrow dispersities (1.09 and 1.13, respectively; Supplementary Fig. 2).

The viologen-iodide (viol-I) polypeptide **6-I** was obtained via $\text{S}_{\text{N}}2$ substitution of halide-containing side chains by the viologen precursor, 1-methyl-[4,4']bipyridylium iodide (MBPI; **1**), prepared via methylation of 4,4'-bipyridine (Fig. 2b). Installation of **1** was initially attempted directly from the chloro-containing polypeptide PCHLG₅₀ **4**, but negligible conversion was observed. The use of an additional activation step to replace the chlorine atoms with iodine via Finkelstein reaction and obtain the iodo-containing polypeptide poly(γ -(6-iodohexyl)-L-glutamate) (PIHLG₅₀; **5**), before the installation step, yielded the viol-I polypeptide with quantitative conversion, as determined by elemental analysis and ^1H NMR spectroscopy (Extended Data Table 2, Supplementary Figs. 14–16). The iodide ion was exchanged to chloride, resulting in the viologen-chloride (viol-Cl) polypeptide **6-Cl**, which was then used for all electrochemical measurements.

For the synthesis of biTEMPO polypeptide, terminal alkynes were incorporated as the side-chain functionality to allow for thiol-yne 'click' chemistry with thiol-decorated TEMPO precursors, followed by deprotection for activation^{31–34}. Methyl-protected methoxyamine derivatives were installed as TEMPO precursors to prevent reduction of the TEMPO-based nitroxide radicals to hydroxylamine in the presence of thiols^{35,36}. Esterification of the methylated 4-hydroxy-TEMPO (MTEMPO; **7**) with 3,3'-dithiodipropionic acid and reduction of the disulfide bond with 1,4-dithiothreitol afforded the thiol-decorated

methyl-protected TEMPO **9**. This thiol was then clicked onto PPLG₅₀ **12** under ultraviolet irradiation in the presence of 2,2-dimethoxy-2-p henylacetophenone (DMPA), followed by oxidative cleavage with *meta*-chloroperoxybenzoic acid (*m*-CPBA) to afford the biTEMPO polypeptide **14**. Elemental analysis suggests that the TEMPO precursors were incorporated with a quantitative amount and that about 18% of the nitroxide radicals were oxidized to the oxoammonium cation (Extended Data Table 2). The efficiency of the final activation step was also evaluated using X-ray photoelectron spectroscopy (Supplementary Figs. 7, 8), indicating that the thioethers (162–164 eV) of **13** were quantitatively oxidized to sulfones (167–169 eV) in **14** and that around 30% of the nitroxide radicals (401 eV) were oxidized to oxoammonium (405 eV). The latter findings were confirmed with ultraviolet–visible spectroscopy (Supplementary Fig. 4) and electron paramagnetic resonance spectroscopy (Supplementary Fig. 5).

We used attenuated total reflectance Fourier transform infrared spectroscopy (Supplementary Fig. 6) and circular dichroism spectroscopy (Supplementary Fig. 3) to confirm the secondary structures of the polypeptides over multiple steps of post-polymerization modification. The viol-Cl and biTEMPO polypeptides both exhibited α -helical conformations, as evidenced by the absorbances in the Fourier transform infrared spectra (Supplementary Fig. 6) at 1,650 cm^{-1} (amide I region) and 1,547 cm^{-1} (amide II region) and by the bands at 208 nm and 222 nm in the circular dichroism spectra (Supplementary Fig. 3). This is expected, because polypeptides can have secondary structures, including helices, sheets, coils and so on^{22,37–39}.

In addition to the redox-active polypeptides, we synthesized small-molecule analogues of the peptide repeat units (Extended Data Fig. 1) to guide structural determination, verify redox potentials and identify degradation products. Synthetic details of these molecules are provided in Supplementary Information (schemes 3 and 4).

Electrochemical characterization

We used cyclic voltammetry of viol-Cl and biTEMPO polypeptide thin films (1 μm thick, 0.5–0.6 mg cm^{-2}) to assess the electrochemical response of the polypeptides in a metal-free electrolyte (0.5 M tetrabutylammonium triflate (TBACF₃SO₃) in propylene carbonate; Fig. 3). The viol-Cl polypeptide exhibited two quasi-reversible redox peaks, at 2.23 V and 2.69 V versus Li/Li⁺ (Fig. 3a). The lower potential (2.23 V) is assigned to the reversible reaction between viologen⁺ (Viol⁺) and viologen⁰ (Viol⁰); the higher potential (2.69 V) is associated with the reversible reaction between viologen²⁺ (Viol²⁺) and Viol^{•+}^{18,20,40}.

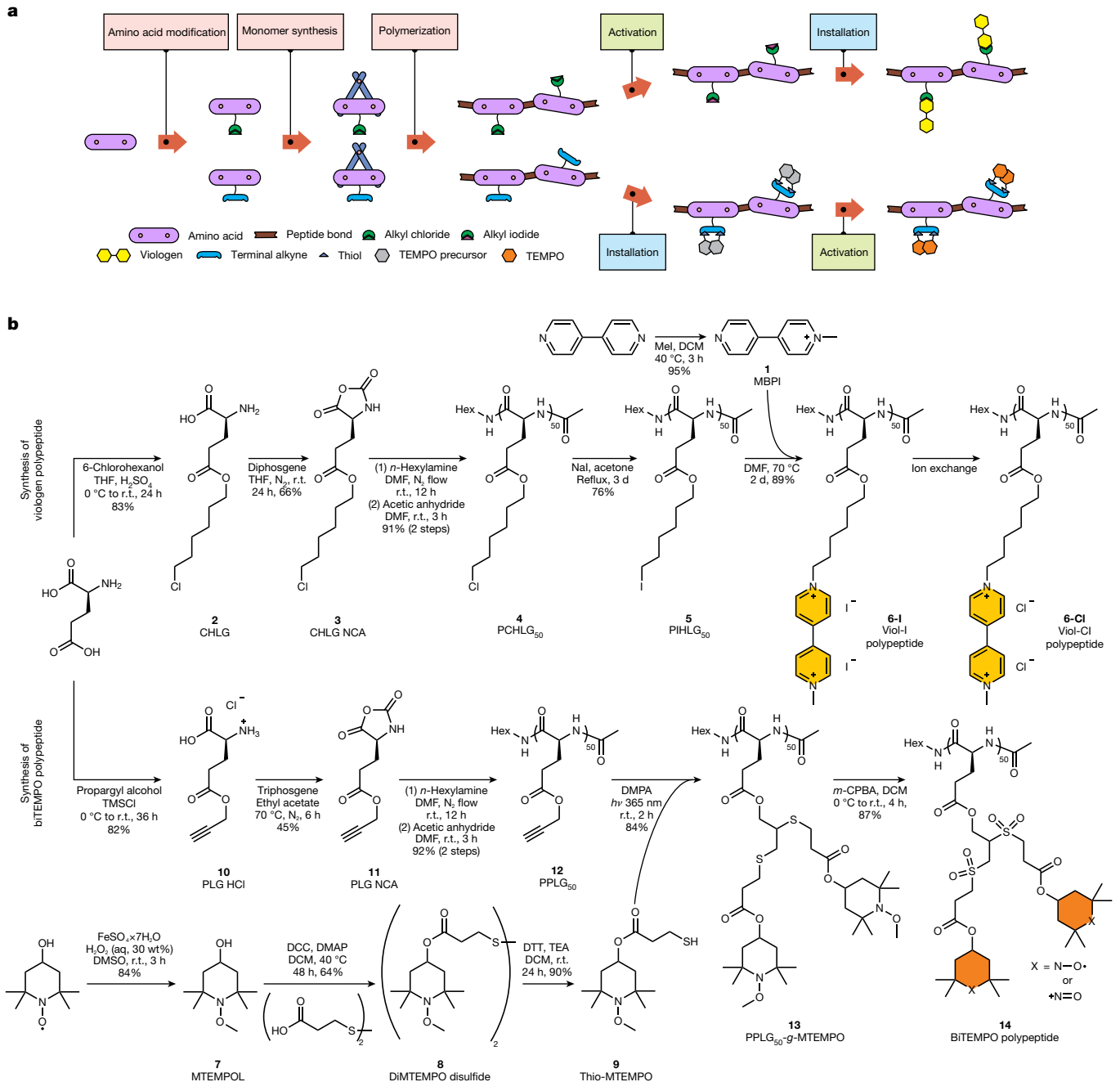


Fig. 2 | Syntheses of redox-active polypeptides. a, b, Synthesis strategy (a) and detailed synthetic schemes (b) for redox-active polypeptides. Modified amino acids are converted into polypeptides, followed by installation of the desired redox-active groups. The viologen group was installed as the anode active material, and the TEMPO nitroxide radical was installed as the cathode

active material. DCC, *N,N'*-dicyclohexylcarbodiimide; DCM, dichloromethane; DMAP, 4-dimethylaminopyridine; DMF, *N,N*-dimethylformamide; DMSO, dimethylsulfoxide; DTT, DL-dithiothreitol; TEA, triethylamine; THF, tetrahydrofuran; TMSCl, trimethylsilyl chloride; r.t., room temperature; *hν*, irradiation.

The biTEMPO polypeptide exhibited one quasi-reversible redox peak, at 3.69 V versus Li/Li^+ , which is associated with the reversible reaction between the nitroxide radical ($\text{N}-\text{O}\cdot$) and oxoammonium cation ($^+\text{N}=\text{O}$; Fig. 3b)¹⁶. The peak current and peak separation for both the viol-Cl and biTEMPO polypeptide thin films scaled with the square-root of the scan rate, which is indicative of a diffusion-limited reaction (Supplementary Figs. 35, 36)^{16,41}. Solution-state cyclic voltammetry of the viologen and biTEMPO analogues (Supplementary Fig. 34) exhibited a similar response.

Next, we fabricated polypeptide composite electrodes (carbon black and polyvinylidene fluoride; 6–7 μm thick, 0.4–0.5 mg polypeptide cm^{-2}) for evaluation in lithium metal half-cells. The theoretical

capacities for the viol-Cl and biTEMPO polypeptides are 118.3 mA h g^{-1} and 71.3 mA h g^{-1} , respectively (Supplementary Information, equation (1)). The viol-Cl polypeptide composite electrode (Fig. 4a–c) exhibited two quasi-reversible redox couples, at 2.13 V and 2.56 V versus Li/Li^+ , and a discharge capacity of 74.2 mA h g^{-1} (per gram of polypeptide) at 1C (the current required to reach full charge in 1 h), which decreased to 68.0 mA h g^{-1} after 30 cycles (91% capacity retention). The biTEMPO polypeptide composite electrode exhibited one quasi-reversible redox peak, at 3.67 V versus Li/Li^+ , and a charge capacity of 16.5 mA h g^{-1} at 1C, which faded to 11.6 mA h g^{-1} after 30 cycles (70% capacity retention; Fig. 4d–f). The main mechanism of capacity fade is dissolution of the polypeptides into the electrolyte, as verified by solution-state cyclic

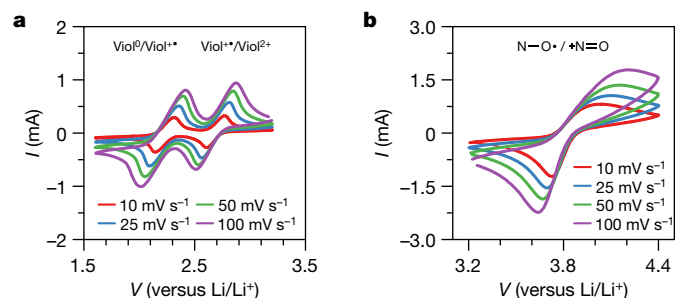


Fig. 3 | Cyclic voltammograms of redox-active polypeptides. **a, b,** Cyclic voltammograms of viol-Cl (**a**) and biTEMPO (**b**) polypeptide thin films on ITO-coated glass substrates in a three-electrode beaker cell configuration. The supporting electrolyte was 0.5 M TBACF₃SO₃ in propylene carbonate. Lithium metal was used as counter and reference electrodes.

voltammetry of the electrolyte after galvanostatic cycling (Supplementary Fig. 37)⁴².

Finally, we prepared metal-free, fully polypeptide-based cells with viol-Cl polypeptide composite anodes and biTEMPO polypeptide

composite cathodes using filter paper soaked with electrolyte as the separator in a sandwich-cell configuration. The theoretical capacity for the fully polypeptide-based cell was calculated to be 44.5 mA h g⁻¹ (per gram of viol-Cl polypeptide; Supplementary Information, equation (2)). Cyclic voltammetry resulted in two pairs of peaks, centred around 1.3 V and 1.6 V, consistent with the difference in redox potentials of the polypeptide composite anode and cathode. Cycling stability of the polypeptide-based battery was determined over 250 cycles of galvanostatic charging at 1C. In the charge–discharge curves, two plateaus occurred, at 1.1 V and 1.6 V (Supplementary Fig. 38). The charge capacity of the full cell at 1C faded from an initial value of 37.8 mA h g⁻¹ (85% theoretical capacity) to 7.5 mA h g⁻¹ after 250 cycles (Fig. 4g–i). The Coulombic efficiency was less than 100% for all cycles, owing to the dissolution of viol-Cl and biTEMPO polypeptides into the electrolyte⁴³. Although dissolution occurred, the post-cycling capacity remained larger than that of the control full cell (without polypeptides), which confirms the activity of the remaining polypeptides even after 250 cycles (Extended Data Fig. 3). There was no visible delamination or morphological change in either composite electrode after 50 cycles (Extended Data Fig. 4). A lithium-ion-based electrolyte battery was tested separately (Supplementary Fig. 39).

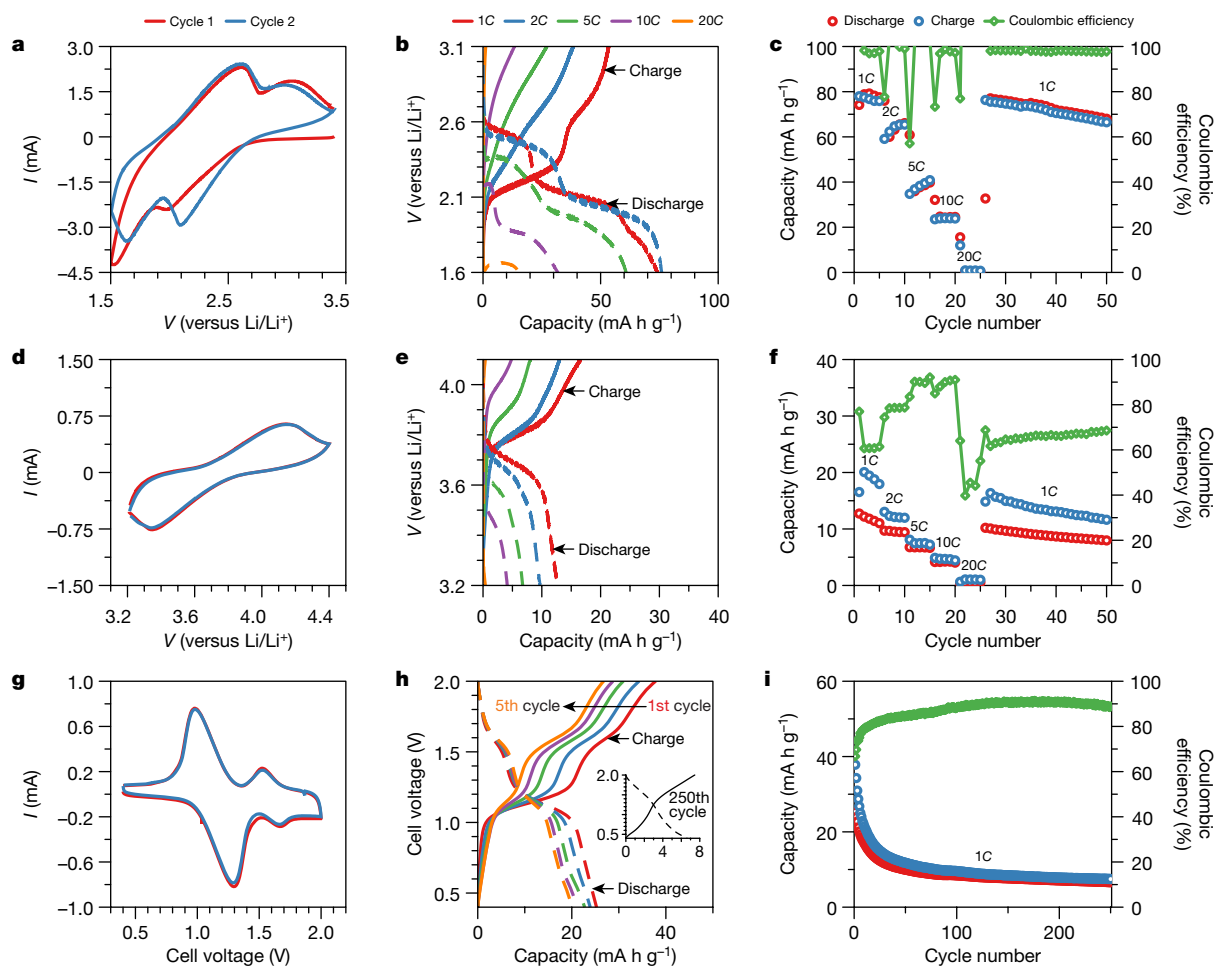


Fig. 4 | Electrochemical response of polypeptide composite half-cells and full cell. **a–i,** Electrochemical characterization of the viol-Cl polypeptide composite half-cell (**a–c**), the biTEMPO polypeptide composite half-cell (**d–f**) and the viol-Cl–biTEMPO polypeptide full cell (**g–i**), including their cyclic voltammograms (**a, d, g**), charge–discharge curves (**b, e, h**; solid, charge; dashed, discharge) and cycling response (**c, f, i**; left axis, charge or discharge capacity; right axis, Coulombic efficiency). For **a–f**, we used a viol-Cl (**a–c**) or biTEMPO (**d–f**) polypeptide composite electrode separated from a lithium

metal reference electrode by filter paper soaked in 0.5 M TBACF₃SO₃ in propylene carbonate. For **g–i**, we used a viol-Cl polypeptide composite electrode separated from a biTEMPO polypeptide composite electrode by filter paper soaked in 0.5 M TBACF₃SO₃ in propylene carbonate. The composite electrodes were composed of 30 wt% active polypeptide, 60 wt% carbon black and 10 wt% polyvinylidene fluoride on ITO-coated glass. In **c** and **f**, the C rates were varied; in **i**, the C rate was constant at 1C.

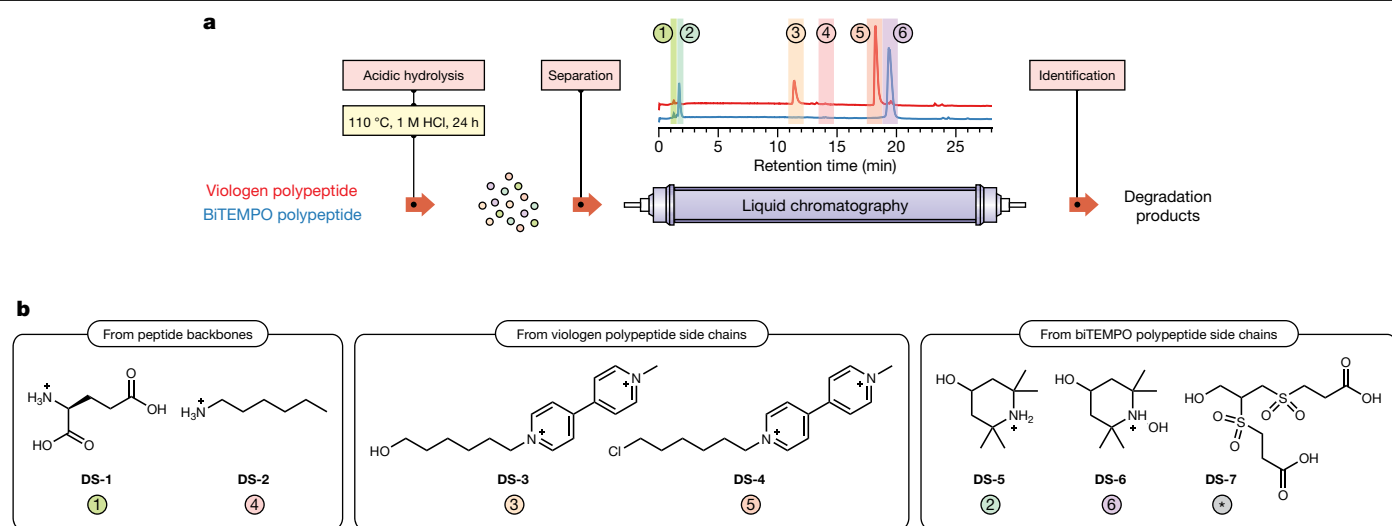


Fig. 5 | Degradation of viologen and biTEMPO polypeptides. Liquid chromatography coupled with high-resolution electrospray ionization mass spectrometry was used to separate and identify the degradation products of the viologen and biTEMPO polypeptides (data from positive-ion mode shown).

On-demand polypeptide degradation

The viologen and biTEMPO polypeptides are designed to contain amide links in the backbone and ester links in the side chains, which are prone to degradation in enzymatic, basic and acidic conditions. Hydrolysis of the viol-I and biTEMPO polypeptides was evaluated under acidic conditions (0.01 M, 1 M and 6 M HCl) at room temperature, 50 °C, 80 °C and 110 °C after 24 h of exposure (Extended Data Table 3). No degradation was observed with 0.01 M HCl at any temperature examined, nor with 1 M or 6 M HCl at room temperature or 50 °C. Partial degradation of the side chains was observed with 1 M and 6 M HCl at 80 °C. Complete degradation of the backbone and side chains for both polypeptides was observed with 1 M and 6 M HCl at 110 °C (Fig. 5). We also investigated the degradation of poly(γ -benzyl-L-glutamate)₅₀ (PBLG₅₀)—a model polypeptide—and the small-molecule viologen and biTEMPO analogues in 1 M HCl at 110 °C to guide the identification of the degradation products generated from the backbones and side chains of the redox-active polypeptides, respectively. We used high-resolution electrospray ionization mass spectrometry (Supplementary Figs. 40–43) to identify the degradation species, which were then verified by ¹H NMR spectroscopy (Supplementary Figs. 48, 49).

The viol-I polypeptide backbone degraded into L-glutamic acid (**DS-1**) and *n*-hexylamine (**DS-2**) in their protonated forms, whereas the side chains were cleaved to yield **DS-3** and chlorinated derivative **DS-4** (Fig. 5, Supplementary Fig. 40). In a similar manner, the biTEMPO polypeptide backbone also generated **DS-1** and **DS-2**, whereas the side chains were cleaved into **DS-5** and **DS-6** (the two degradation products of 4-hydroxy-TEMPO; Fig. 5, Supplementary Fig. 42), in addition to **DS-7** (the linker between glutamate units and TEMPO moieties; Supplementary Fig. 43). ¹H NMR spectra suggest that L-glutamic acid was regenerated in near-quantitative amounts for both the viol-I and biTEMPO polypeptides (Supplementary Figs. 48, 49).

We used liquid chromatography to separate degradation products of the redox-active polypeptides, their small-molecule analogues and the model polypeptide backbone PBLG₅₀ (Supplementary Figs. 44–47). The order (from first to last) of elution for the degraded viol-I polypeptide in positive-ion mode was **DS-1**, **DS-3**, **DS-2** and then **DS-4**. Similarly, the order of elution for the degraded biTEMPO polypeptide was **DS-1**, **DS-5**, **DS-2** and then **DS-6**. The linker **DS-7** was detected separately in the negative-ion mode (Supplementary Fig. 47). Together, these results demonstrate the on-demand degradation of the polypeptides, and the identification and separation of the degradation products.

Reconstructing the polymers from the degradation products would be the ultimate demonstration of recyclability. We found that the primary issue with achieving this was separating the degradation products on a scale large enough for subsequent reconstruction into the original polymers. In principle, the redox-active polymers would be reconstituted by the following: (1) the regenerated glutamic acid could be fed directly back into the syntheses of the viologen and biTEMPO polypeptides as primary synthons; (2) the 4-OH-TEMPO radicals could be retrieved upon separation, neutralization and oxidation of the degradation products **DS-5** and **DS-6**, then fed into the synthetic route of the biTEMPO polypeptide; and (3) the degradation product **DS-3** of the viologen polypeptide side chains could be conjugated with poly(L-glutamates) to regenerate the viologen polypeptide. Alternatively, a milder degradation process, for instance, enzymatic breakdown, might provide a simpler route to a full cycle of recyclability.

Cell viability study

We conducted cell viability testing with preosteoblast (MC3T3) cells, mouse fibroblast (NIH/3T3) cells and bovine coronary venular endothelial (CVE) cells to evaluate the toxicity of the polypeptides, their repeat-unit analogues and their degradation products. In general, the viol-I polypeptide was toxic towards MC3T3 and fibroblast cells, owing to its polycationic nature, whereas the biTEMPO polypeptide was deemed non-toxic towards all cell lines examined. The degradation products of viol-I polypeptide had lower toxicity effects than did the original polypeptide towards all three cell lines tested. The degradation products of the biTEMPO polypeptides exhibited no toxicity. A summary of the effect on cell viability of the polypeptides, small-molecule analogues and their degradation products are provided in Extended Data Figs. 5–7 and Supplementary Figs. 50, 51.

Summary

We have designed a metal-free, all-polypeptide organic radical battery comprising redox-active amino-acid macromolecules that degrade on demand. This concept represents a first step towards sustainable, recyclable batteries and minimizing global dependence on strategic metals. Viologen and biTEMPO polypeptide anodes and cathodes, respectively, were synthesized via ring-opening polymerization of highly reactive cyclic *N*-carboxyanhydrides, followed by sequential post-polymerization modifications to incorporate the redox-active

groups. The polypeptide battery reached a maximum charge capacity of 37.8 mA h g^{-1} (theoretical capacity, 44.5 mA h g^{-1}). The active components degraded on demand in the presence of acid to regenerate the starting amino acids and other building blocks. Looking forwards, the main challenges are preventing dissolution of the active material and boosting the overall cell capacity. Future studies should focus on preventing dissolution of the polypeptides by crosslinking⁴⁴, by post-processing modification⁴⁵ or by taking advantage of the solubility of the polypeptides in flow battery cells.

Online content

Any methods, additional references, Nature Research reporting summaries, source data, extended data, supplementary information, acknowledgements, peer review information; details of author contributions and competing interests; and statements of data and code availability are available at <https://doi.org/10.1038/s41586-021-03399-1>.

- Lopez, J., Mackanic, D. G., Cui, Y. & Bao, Z. Designing polymers for advanced battery chemistries. *Nat. Rev. Mater.* **4**, 312–330 (2019).
- Turcheniuk, K., Bondarev, D., Singhal, V. & Yushin, G. Ten years left to redesign lithium-ion batteries. *Nature* **559**, 467–470 (2018).
- Zeng, X., Li, J. & Singh, N. Recycling of spent lithium-ion battery: a critical review. *Crit. Rev. Environ. Sci. Technol.* **44**, 1129–1165 (2014).
- Olivetti, E. A., Ceder, G., Gaustad, G. & Fu, X. Lithium-ion battery supply chain considerations: analysis of potential bottlenecks in critical metals. *Joule* **1**, 229–243 (2017).
- Wild, A., Strumpf, M., Häupler, B., Hager, M. D. & Schubert, U. S. All-organic battery composed of thianthrene- and TCAQ-based polymers. *Adv. Energy Mater.* **7**, 1601415 (2017).
- Banza Lubaba Nkulu, C. et al. Sustainability of artisanal mining of cobalt in DR Congo. *Nat. Sustain.* **1**, 495–504 (2018).
- Koshika, K., Chikushi, N., Sano, N., Oyaizu, K. & Nishide, H. A TEMPO-substituted polyacrylamide as a new cathode material: an organic rechargeable device composed of polymer electrodes and aqueous electrolyte. *Green Chem.* **12**, 1573–1575 (2010).
- Esquivel, J. P. et al. A metal-free and biotically degradable battery for portable single-use applications. *Adv. Energy Mater.* **7**, 1700275 (2017).
- Friebe, C., Lex-Balducci, A. & Schubert, U. S. Sustainable energy storage: recent trends and developments toward fully organic batteries. *ChemSusChem* **12**, 4093 (2019).
- Janoschka, T., Hager, M. D. & Schubert, U. S. Powering up the future: radical polymers for battery applications. *Adv. Mater.* **24**, 6397–6409 (2012).
- Kim, J., Kim, J. H. & Ariga, K. Redox-active polymers for energy storage nanoarchitectonics. *Joule* **1**, 739–768 (2017).
- Tomlinson, E. P., Hay, M. E. & Boudouris, B. W. Radical polymers and their application to organic electronic devices. *Macromolecules* **47**, 6145–6158 (2014).
- Lutkenhaus, J. A radical advance for conducting polymers. *Science* **359**, 1334–1335 (2018).
- Joo, Y., Agarkar, V., Sung, S. H., Savoie, B. M. & Boudouris, B. W. A nonconjugated radical polymer glass with high electrical conductivity. *Science* **359**, 1391–1395 (2018).
- Coates, G. W. & Getzler, Y. D. Y. L. Chemical recycling to monomer for an ideal, circular polymer economy. *Nat. Rev. Mater.* **5**, 501–516 (2020).
- Muench, S. et al. Polymer-based organic batteries. *Chem. Rev.* **116**, 9438–9484 (2016).
- Zhang, K., Monteiro, M. J. & Jia, Z. Stable organic radical polymers: synthesis and applications. *Polym. Chem.* **7**, 5589–5614 (2016).
- Janoschka, T. et al. An aqueous, polymer-based redox-flow battery using non-corrosive, safe, and low-cost materials. *Nature* **527**, 78–81 (2015).
- Koshika, K., Sano, N., Oyaizu, K. & Nishide, H. An aqueous, electrolyte-type, rechargeable device utilizing a hydrophilic radical polymer-cathode. *Macromol. Chem. Phys.* **210**, 1989–1995 (2009).
- Sano, N. et al. Polyviologen hydrogel with high-rate capability for anodes toward an aqueous electrolyte-type and organic-based rechargeable device. *ACS Appl. Mater. Interfaces* **5**, 1355–1361 (2013).
- Suga, T., Ohshiro, H., Sugita, S., Oyaizu, K. & Nishide, H. Emerging n-type redox-active radical polymer for a totally organic polymer-based rechargeable Battery. *Adv. Mater.* **21**, 1627–1630 (2009).
- Suga, T., Sugita, S., Ohshiro, H., Oyaizu, K. & Nishide, H. p- and n-type bipolar redox-active radical polymer: toward totally organic polymer-based rechargeable devices with variable configuration. *Adv. Mater.* **23**, 751–754 (2011).
- Oka, K., Kato, R., Oyaizu, K. & Nishide, H. Poly(vinylidenebenzothioophenylsulfone): its redox capability at very negative potential toward an all-organic rechargeable device with high-energy density. *Adv. Funct. Mater.* **28**, 1805858 (2018).
- Qu, J. et al. Synthesis and properties of DNA complexes containing 2,2,6,6-tetramethyl-1-piperidinyloxy (TEMPO) moieties as organic radical battery materials. *Chemistry* **14**, 3250–3259 (2008).
- Ibe, T., Frings, R. B., Lachowicz, A., Kyo, S. & Nishide, H. Nitroxide polymer networks formed by Michael addition: on site-cured electrode-active organic coating. *Chem. Commun.* **46**, 3475–3477 (2010).
- Qu, J. et al. Helical polyacetylenes carrying 2,2,6,6-tetramethyl-1-piperidinyloxy and 2,2,5,5-tetramethyl-1-pyrrolidinyloxy moieties: their synthesis, properties, and function. *J. Polym. Sci. A* **45**, 5431–5445 (2007).
- Otaki, M. & Goto, H. Helical spin polymer with magneto-electro-optical activity. *Macromolecules* **52**, 3199–3209 (2019).
- Hatakeyama-Sato, K., Wakamatsu, H., Katagiri, R., Oyaizu, K. & Nishide, H. An ultrahigh output rechargeable electrode of a hydrophilic radical polymer/nanocarbon hybrid with an exceptionally large current density beyond 1 A cm^{-2} . *Adv. Mater.* **30**, 1800900 (2018).
- Hiejima, T. & Kaneko, J. Spiral configuration of nitroxide radicals along the polypeptide helix and their magnetic properties. *Macromolecules* **46**, 1713–1722 (2013).
- Belshaw, P. J., Mzengeza, S. & Lajoie, G. A. Chlorotrimethylsilane mediated formation of ω -allyl esters of aspartic and glutamic acids. *Synth. Commun.* **20**, 3157–3160 (1990).
- Deming, T. J. Synthesis of side-chain modified polypeptides. *Chem. Rev.* **116**, 786–808 (2016).
- Fan, J. et al. Construction of a versatile and functional nanoparticle platform derived from a helical diblock copolypeptide-based biomimetic polymer. *Polym. Chem.* **5**, 3977–3981 (2014).
- Engler, A. C., Lee, H.-i. & Hammond, P. T. Highly efficient “grafting onto” a polypeptide backbone using click chemistry. *Angew. Chem. Int. Ed.* **48**, 9334–9338 (2009).
- Hoyle, C. E. & Bowman, C. N. Thiol-ene click chemistry. *Angew. Chem. Int. Ed.* **49**, 1540–1573 (2010).
- Hansen, K.-A. et al. A methoxyamine-protecting group for organic radical battery materials—an alternative approach. *ChemSusChem* **13**, 2386 (2020).
- Galbo, J. P. Process for preparing N-methoxy derivatives of 4-hydroxy-2,2,6,6-tetramethylpiperidine and 2,2,6,6-tetramethyl-4-piperidone. US patent 5374729A (1994).
- Deming, T. J. Noodle gels for cells. *Nat. Mater.* **9**, 535–536 (2010).
- Lalatsa, A., Schätzlein, A. G., Mazza, M., Le, T. B. H. & Uchegbu, I. F. Amphiphilic poly(L-amino acids) — new materials for drug delivery. *J. Control. Release* **161**, 523–536 (2012).
- Matson, J. B. & Stupp, S. I. Self-assembling peptide scaffolds for regenerative medicine. *Chem. Commun.* **48**, 26–33 (2012).
- Shpilevaya, I. & Foord, J. S. Electrochemistry of methyl viologen and anthraquinonedisulfonate at diamond and diamond powder electrodes: the influence of surface chemistry. *Electroanalysis* **26**, 2088–2099 (2014).
- Bard, A. J. & Faulkner, L. R. *Electrochemical Methods: Fundamentals and Applications* 2nd edn, Ch. 6 (Wiley, 2000).
- Bugnon, L., Morton, C. J. H., Novak, P., Vetter, J. & Nesvadba, P. Synthesis of poly(4-methacryloyloxy-TEMPO) via group-transfer polymerization and its evaluation in organic radical battery. *Chem. Mater.* **19**, 2910–2914 (2007).
- Janoschka, T. et al. Reactive inkjet printing of cathodes for organic radical batteries. *Adv. Energy Mater.* **3**, 1025–1028 (2013).
- Vlad, A., Rolland, J., Hauffman, G., Ernould, B. & Gohy, J.-F. Melt-polymerization of TEMPO methacrylates with nano carbons enables superior battery materials. *ChemSusChem* **8**, 1692–1696 (2015).
- Lutkenhaus, J. et al. Solution-processable thermally crosslinked organic radical polymer battery cathodes. *ChemSusChem* **13**, 2371 (2020).

Publisher's note Springer Nature remains neutral with regard to jurisdictional claims in published maps and institutional affiliations.

© The Author(s), under exclusive licence to Springer Nature Limited 2021

Methods

Reagents

Acetonitrile (MeCN), 3,3-dithiodipropionic acid, 4,4'-dipyridine, *meta*-chloroperoxybenzoic acid (*m*-CPBA; 77% purity), dichloromethane (DCM), *N,N'*-dicyclohexylcarbodiimide (DCC), 4-dimethylaminopyridine (DMAP), 2,2-dimethoxy-2-*p*-phenylacetophenone (DMPA), *N,N*-dimethylformamide (DMF), dimethylsulfoxide (DMSO), 4-hydroxy-2,2,6,6-tetramethylpiperidine-1-oxyl (4-OH-TEMPO, TEMPOL), diphosgene, hexanes, *n*-hexylamine, hydrocinnamic acid, iodomethane, iron(II) sulfate heptahydrate (FeSO₄·7H₂O), L-glutamic acid, methanol, propargyl alcohol, sodium iodide (NaI), triethylamine (TEA), trifluoroethanol (TFE), trimethylsilyl chloride (TMSCl) and triphosgene were purchased from Sigma-Aldrich. DL-Dithiothreitol (DTT) was purchased from Tokyo Chemical Industry. 6-Chloro-1-hexanol and acetic anhydride were purchased from Alfa-Aesar. All reagents were used as received, except for propargyl alcohol, which was distilled under an atmosphere of N₂ before use. Ultrapure water was collected from a Milli-Q integral water purification system (18 MΩ cm). Lithium triflate (LiCF₃SO₃), tetrabutylammonium triflate (TBACF₃SO₃), methanol, *N*-methyl-2-pyrrolidinone (NMP) and propylene carbonate (PC) were purchased from Sigma-Aldrich. DCM and chloroform were purchased from VWR. Super P carbon black (CB) was purchased from TIMCAL Graphite & Carbon. Polyvinylidene fluoride (PVDF; 600,000 g mol⁻¹) was purchased from MTI. ITO-coated glass substrates were purchased from Delta Technologies, and cleaned by subsequent sonication in soap water, ultrapure water, acetone and isopropyl alcohol, followed by drying with N₂ and ozone plasma treatment for 10 min. Lithium metal was purchased from Alfa-Aesar.

Chemical characterization

Attenuated total reflectance Fourier transform infrared (ATR-FTIR) spectra were recorded for powder samples on an infrared Prestige 21 system (Shimadzu) and analysed using IRsolution version 1.40 software. Circular dichroism spectra of the polymer solutions were recorded on a Chirascan circular dichroism spectrometer from Applied Photophysics (Leatherhead) equipped with a 150-W xenon arc lamp. The concentration of the biTEMPO polypeptide solution was 0.1 mg ml⁻¹ in MeCN. The viol-Cl polypeptide solution was prepared by adding 2.5 μl of 40 mg ml⁻¹ in H₂O into 1 ml of MeCN. Circular dichroism spectra were acquired between 180 nm and 280 nm, using a wavelength step of 1.0 nm, in a quartz cell with a path length of 1.0 cm, and analysed using Pro-Data version 5 software. Electron paramagnetic resonance spectra were recorded on an X-Band Bruker EMS spectrometer with an Oxford ESR900 liquid helium cryostat. X-ray photoelectron spectroscopy (XPS) measurements of the polypeptide and analogue thin films were recorded on an Omicron XPS system with Argus detector using Omicron's 400 dual Mg/Al X-ray source. The thin films were prepared by drop-casting 300 μl of each polymer or analogue solution (4 mg ml⁻¹ in CHCl₃) on ITO-coated glass substrates. After drop-casting, the thin films were dried at ambient conditions for 24 h, followed by drying under vacuum at room temperature for 24 h before XPS measurements. ¹H and ¹³C NMR spectra were recorded on a Bruker 400 spectrometer. Chemical shifts were referenced to the solvent resonance signals. Elemental analysis was conducted using the service provided by Robertson Micro-lit Laboratories. UV-Vis spectra were collected in 1-nm increments from 800 nm to 300 nm using a Hitachi U-4100 UV-Vis-NIR spectrophotometer (341-F). The 4-OH-TEMPO calibration curve was constructed by varying the concentration from 0.01 M to 0.04 M in chloroform. The biTEMPO polypeptide sample was prepared at a concentration of 0.03 M (repeat-unit basis) in chloroform and the radical content was calculated at 462 nm. High-resolution electrospray ionization mass spectrometry (ESI-HRMS) experiments were performed using a Thermo Scientific Q Exactive Focus in positive and negative mode. The sample was injected into a 10-μl loop and methanol was used as a

mobile phase at a flow rate of 100 μl min⁻¹. The Q Exactive Focus HESI source was operated in full mass spectroscopy in positive mode. The mass resolution was tuned to 70,000 full-width at half-maximum at *m/z* 200. The spray voltage was set to 3.75 kV for positive mode and 3.3 kV for negative mode; the sheath gas and auxiliary gas flow rates were set to 7 and 0 arbitrary units, respectively. The transfer capillary temperature was held at 250 °C and the S-Lens radio-frequency level was set at 50 V. Exactive Series 2.8 SP1/Xcalibur version 4.0 software was used for data acquisition and processing.

Thermal analysis

Thermogravimetric analysis was performed under nitrogen atmosphere using a Mettler–Toledo model TGA 2 with a heating rate of 10 °C min⁻¹. Measurements were analysed using Mettler–Toledo STAR^e version 7.01 software. Glass transition temperatures were measured by modulated differential scanning calorimetry on a Q200 DSC (TA Instruments) with a heat-cool-heat cycle. The samples were ramped from -40 °C to 200 °C at a rate of 5 °C min⁻¹ with amplitude of 1.272 °C for a period of 60 s with nitrogen purge at 50 ml min⁻¹. The glass transition temperature was taken as the inflection point of the second heating cycle.

Electrochemical characterization

Polypeptide thin films were prepared by drop-casting 300 μl of the polypeptide solution onto clean ITO-coated glass substrates. The polypeptide solution was composed of 4 mg of polypeptide in 1 ml of MeOH/H₂O (1/1 v/v) for viol-Cl polypeptide or CHCl₃ for biTEMPO polypeptide. After drop-casting, the thin films were dried at ambient conditions for 24 h, followed by drying under vacuum at room temperature for 24 h before electrochemical testing. Composite electrodes for both polymers were fabricated by preparing a solution of CB (60 wt%), biTEMPO polypeptide or viol-Cl polypeptide (30 wt%) and PVDF binder polymer (10 wt%) in NMP (1 ml). 300 μl of the slurry was then drop-cast onto a clean ITO-coated glass substrate. After drop-casting the slurry onto the substrates, the electrodes were dried at 40 °C under ambient pressure for two days before drying under vacuum at room temperature for 24 h. After drying, the electrode thickness was determined with a TESA μ-HITE instrument. All electrochemical measurements were performed in an argon-filled glovebox with a Solartron Electrochemical Interface 1287 potentiostat/galvanostat unless otherwise noted.

The polypeptide thin films on ITO-coated glass substrates were used in a three-electrode beaker cell as the working electrode with lithium metal counter and reference electrodes, and 20 ml of 0.5 M TBACF₃SO₃ or LiCF₃SO₃ in PC for the electrolyte. The thin films were conditioned using three cyclic voltammetry cycles at 10 mV s⁻¹ followed by cyclic voltammetry at different scan rates (10 mV s⁻¹, 25 mV s⁻¹, 50 mV s⁻¹ or 100 mV s⁻¹).

The composite electrodes were used in a half sandwich cell as working electrodes, with a lithium metal reference electrode and filter paper pre-soaked with 0.5 M TBACF₃SO₃ or LiCF₃SO₃ in PC as the separator (Extended Data Fig. 2a). Cyclic voltammetry (10 mV s⁻¹) and galvanostatic charge-discharge (five cycles each at 1C, 2C, 5C, 10C and 20C followed by 25 cycles at 1C) were performed. The current (*I*, mA) for each *C* rate was calculated using the theoretical capacity and coated mass (*X*, g polypeptide) of the polypeptide. For example, for a biTEMPO composite electrode at 1C: $I/[mA] = 71.3 [mA h (g \text{ biTEMPO})^{-1}] \times X [g \text{ biTEMPO}] \times 1 [h^{-1}]$.

All polypeptide electrochemical sandwich cells were assembled with viol-Cl polypeptide composite anodes, biTEMPO polypeptide composite cathodes and electrolyte-soaked filter-paper separators (Extended Data Fig. 2b). The electrolyte was 0.5 M TBACF₃SO₃ or LiCF₃SO₃ in PC. Before sandwich-cell assembly, the viol-Cl polypeptide electrodes were conditioned with three cyclic voltammetry cycles at 10 mV s⁻¹ in a three-electrode beaker cell containing 0.5 M TBACF₃SO₃ or LiCF₃SO₃ in PC electrolyte with lithium metal counter and reference electrodes.

Article

Cyclic voltammetry of the full sandwich cell was conducted at 10 mV s⁻¹ before galvanostatic charge–discharge at 1C for 250 cycles. We also conducted electrochemical characterization of the polypeptides as composite electrodes in three-electrode cell configuration (Supplementary Tables 1, 2).

Degradation study

Viologen polypeptide and biTEMPO polypeptide were exposed to 0.01 M, 1 M and 6 M HCl at 2.5 mg ml⁻¹ over 24 h at room temperature, 50 °C, 80 °C and 110 °C. PBLG₅₀, small-molecule analogues of the polypeptides and 4-OH-TEMPO were hydrolysed at 2.5 mg ml⁻¹ with 1 M HCl over 24 h at 110 °C to guide the breakdown of the polypeptide backbones and sidechains.

We analysed the degradation products using ESI-HRMS and liquid chromatography coupled with ESI-HRMS, using a Thermo Scientific Ultimate 3000 Series LC coupled with a Thermo Scientific Qexactive Focus mass spectrometer. A Scherzo SM-C18 (150 × 2 mm, 3 μm particle size) column (Imtakt) was used for chromatographic separation. The mobile phase consisted of 20 mM NH₄HCO₂ in H₂O (eluent A) and 100 mM NH₄HCO₂ in H₂O/MeCN (1/1 v/v; eluent B). The flow rate was set at 0.3 ml min⁻¹ and 10 μl of each sample was injected. The column compartment was held at 30 °C. Chromatographic gradient elution was set by first equilibrating the column for 3 min at 5% eluent B. Eluent B was then gradually increased from 5% to 100% for 18 min and held at 100% for 3 min. The eluent was then set to the initial mobile phase condition (5% eluent B) in 0.1 min and kept constant for 3 min. The conditions for the mass spectrometry were similar to those described above, except that the capillary temperature was set to 350 °C and the sheath gas and auxiliary gas flow rates were set to 35 and 8 arbitrary units, respectively.

Toxicity study

Preosteoblast (MC3T3) cells were purchased from ATCC and cultured in Alpha Minimum Essential Medium, with ribonucleosides but without ascorbic acid, supplemented with 10% fetal bovine serum (FBS) and 1% penicillin-streptomycin (Millipore Sigma), with final concentrations of 100 U ml⁻¹ penicillin and 100 μg ml⁻¹ streptomycin. Bovine CVE cells were gifted by Cynthia J. Meinger and Andreea Trache at Texas A&M Health Science Center. CVE cells were cultured in Dulbecco's Modified Eagle Medium Nutrient Mixture F-12 (DMEM/F-12) supplemented with 10% FBS and 1% antibiotic (final concentration: 100 U ml⁻¹ penicillin, 100 U ml⁻¹ streptomycin, 0.25 mg ml⁻¹ amphotericin B (Lonza) and 20 U ml⁻¹ heparin (Midwest Vet Supply)). Mouse fibroblast (NIH/3T3) cells were purchased from ATCC and cultured in DMEM supplemented with 10% FBS and 1% penicillin-streptomycin (Millipore Sigma), with final concentrations of 100 U ml⁻¹ penicillin and 100 μg ml⁻¹ streptomycin. Reagents were purchased from Thermo Fisher Scientific unless otherwise stated.

CellTiter 96 AQ One Solution Cell Proliferation Assay was purchased from Promega and used without modification, as described previously⁴⁶. Cells were grown to confluency. Viologen polypeptide, biTEMPO polypeptide, viologen analogue and biTEMPO analogue were dissolved in sterile DMSO at 10 mg ml⁻¹, whereas their degraded products were dissolved in sterile PBS buffer pH 7.6 at similar concentration. All testing substances were filtered via sterile syringe filter and added to the cells at concentrations indicated in Extended Data Figs. 5–7 and Supplementary Figs. 50, 51 (0.05–100 μg ml⁻¹). Control cells were incubated with fresh culture medium. The plates were then incubated at 37 °C for 72 h. Subsequently, a 20-μl aliquot of MTS reagent was added to each well and incubated for another 2 h. The absorbance was recorded at 490 nm. Cell viability below 50% was considered indicative of cytotoxicity. Data are expressed as mean ± s.d. of three determinations.

The viologen polypeptide exhibited no cytotoxicity towards CVE cells (IC₅₀ > 100 μg ml⁻¹), but showed cytotoxicity towards MC3T3

cells (IC₅₀ = 1.52 μg ml⁻¹) and fibroblasts (IC₅₀ = 2.68 μg ml⁻¹; Extended Data Fig. 5). By contrast, the viologen analogue revealed no loss in cell viability towards MC3T3 and CVE cells (IC₅₀ > 100 μg ml⁻¹), but revealed some adverse effect on fibroblasts (IC₅₀ = 34.9 μg ml⁻¹; Supplementary Fig. 50). This difference may originate from the polycationic nature of the viologen polypeptide, which promotes cell-membrane disruption and cell death. The higher IC₅₀ values against CVE cells may be complicated by the addition of heparin to the cell media, which is polyanionic and may complex to different extents with the cationic viologen-based polypeptides, analogues and degradation products. The biTEMPO polypeptide exhibited little to no cytotoxicity towards all three cell lines (IC₅₀ = 88.9 μg ml⁻¹, IC₅₀ = 63.2 μg ml⁻¹ and IC₅₀ > 100 μg ml⁻¹ towards MC3T3, fibroblast and CVE cells, respectively; Extended Data Fig. 5). Whereas the small-molecule biTEMPO analogue exhibited limited cytotoxicity towards MC3T3 (IC₅₀ = 55.9 μg ml⁻¹) and fibroblast (47.3 μg ml⁻¹) cells, it expressed a greater effect towards CVE cells (IC₅₀ = 17.3 μg ml⁻¹; Supplementary Fig. 50).

In general, the degradation products for both polypeptides exhibited lower toxic effects compared to their original, undegraded forms and similar effects to the degradation products of their small-molecule analogues (Extended Data Fig. 6, Supplementary Fig. 51). The viologen polypeptide degradation products expressed lower cytotoxicity at higher IC₅₀ towards MC3T3 and fibroblast cells (IC₅₀ = 31.3 μg ml⁻¹ and 17.9 μg ml⁻¹, respectively), compared to the original polycationic viologen polypeptide (IC₅₀ = 1.52 μg ml⁻¹ and 2.52 μg ml⁻¹, respectively). The toxicity for the degradation products being at much lower concentration towards CVE cells (IC₅₀ = 33.6 μg ml⁻¹ compared to IC₅₀ > 100 μg ml⁻¹ of the original viologen polypeptide) may again be complicated by the increased positive-charge density of the degradation compounds, in addition to the effect of heparin in the cell media (Extended Data Fig. 6). The degradation products of biTEMPO polypeptide and biTEMPO analogue showed no toxicity towards all three cell lines (IC₅₀ > 100 μg ml⁻¹; Extended Data Fig. 6, Supplementary Fig. S51).

Data availability

All data generated or analysed during this study are included in paper and its Supplementary Information. Source data are provided with this paper.

46. Elsabahy, M., Samarajeewa, S., Raymond, J. E., Clark, C. & Wooley, K. L. Shell-crosslinked knedel-like nanoparticles induce lower immunotoxicity than their non-crosslinked analogs. *J. Mater. Chem. B* **1**, 5241–5255 (2013).

Acknowledgements This work was financially supported by the National Science Foundation (DMR-1507429, DMR-1905818, CHE-2003771 and DMR-1629094; K.L.W. and T.P.N.; synthesis and structural characterization), the Welch Foundation (A-0001, K.L.W.; A-1717, C.-H.Y.) and the US Department of Energy Office of Science (DE-SC0014006; J.L.L. and A.D.E.; electrochemical measurements). A.D.E. acknowledges support by a National Science Foundation Graduate Research Fellowship.

Author contributions T.P.N. and A.D.E. contributed equally to this work. T.P.N., A.D.E., J.L.L. and K.L.W. developed the study. T.P.N. synthesized and structurally characterized the viologen and biTEMPO polypeptides. A.D.E. performed the electrochemical characterization of the materials. XPS and scanning electron microscopy data were obtained by N.K., electron paramagnetic resonance by S.W. and thermal characterization by A.D.E. and D.K.T. The degradation study was done by T.P.N., with help from Y.H.R. for mass spectrometry. The cytotoxicity study was done by S.K. and S.-M.L. The manuscript was written by T.P.N. and A.D.E., with help from J.F., R.A.L., X.H., L.S., C.-H.Y., J.L.L. and K.L.W.

Competing interests The authors declare no competing interests.

Additional information

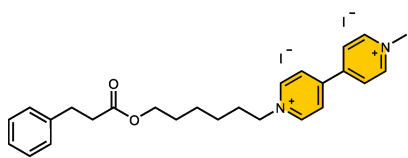
Supplementary information The online version contains supplementary material available at <https://doi.org/10.1038/s41586-021-03399-1>.

Correspondence and requests for materials should be addressed to J.L.L. or K.L.W.

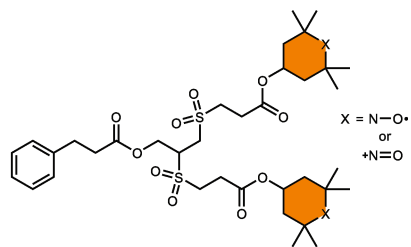
Peer review information Nature thanks Jung Ho Kim, David Mercereyes and Ulrich Schubert for their contribution to the peer review of this work.

Reprints and permissions information is available at <http://www.nature.com/reprints>.

Viologen Analogue

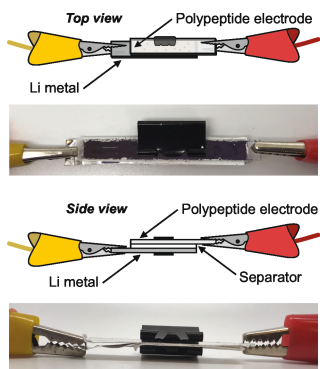


BiTEMPO Analogue

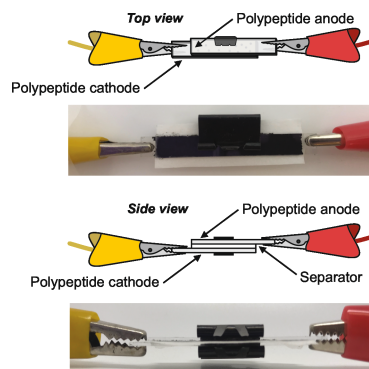


Extended Data Fig. 1 | Molecular structures of viologen and biTEMPO analogues.

A Half Sandwich Cell



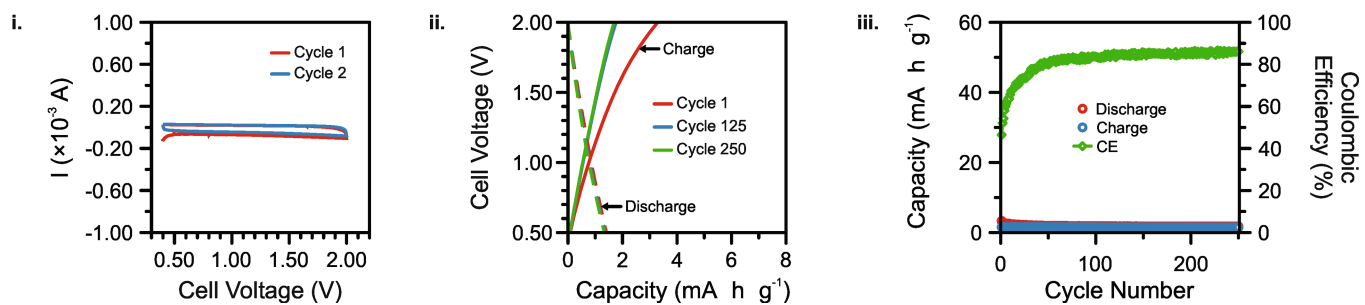
B Full Sandwich Cell



Extended Data Fig. 2 | Electrochemistry assemblies. **a**, The half sandwich cell: viol-Cl or biTEMPO polypeptide composite working electrode and lithium metal reference electrode, with a filter-paper separator. **b**, The full sandwich

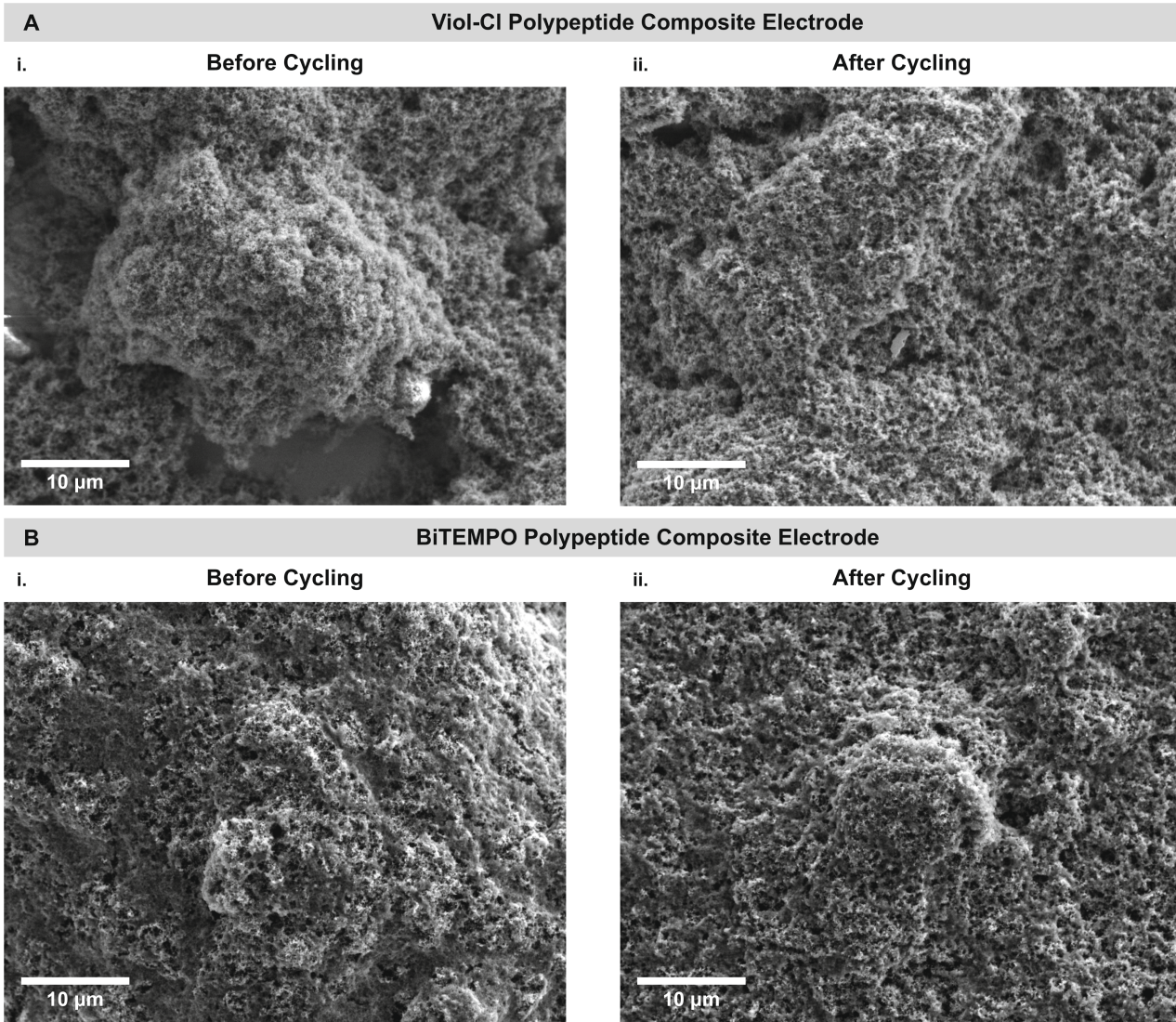
cell: viol-Cl polypeptide composite working electrode and biTEMPO polypeptide composite reference electrode, with a filter-paper separator.

CB + PVDF Electrode | CB + PVDF Electrode



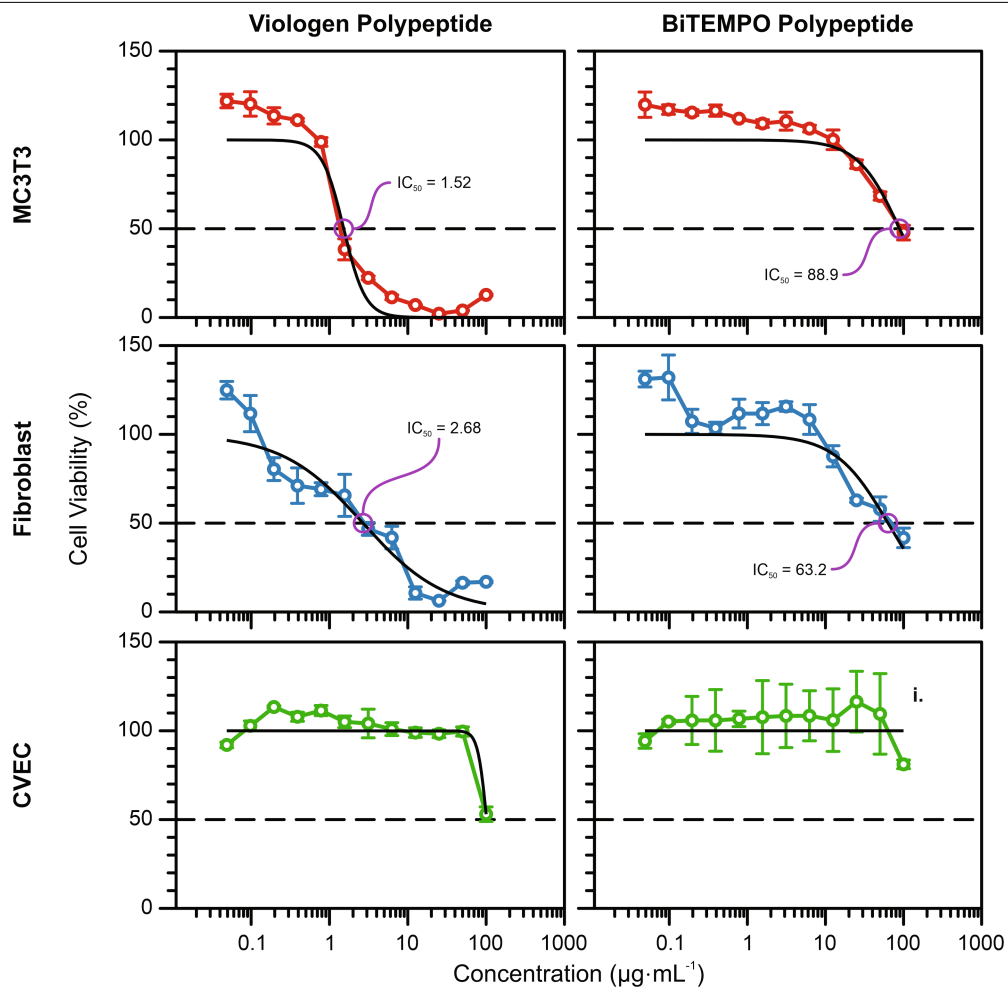
Extended Data Fig. 3 | Electrochemical performance of full cell without polypeptide active material as a control. Electrochemical characterization of a PVDF + CB symmetric full cell is shown, including cyclic voltammograms (i), charge-discharge curves (ii) and cycling response at 1C (iii) (PVDF + CB composite electrode, 0.5 M TBACF₃SO₃ in PC and filter paper, PVDF + CB

composite electrode). The composite electrodes were cast in an identical manner to the polypeptide composite electrodes, with a composition of 86 wt% CB and 14 wt% PVDF on ITO-coated glass substrates. After 250 cycles, the capacity was 1.7 mA h g^{-1} , whereas the capacity of the polypeptide-based full cell was 7.5 mA h g^{-1} (Fig. 4g-i).

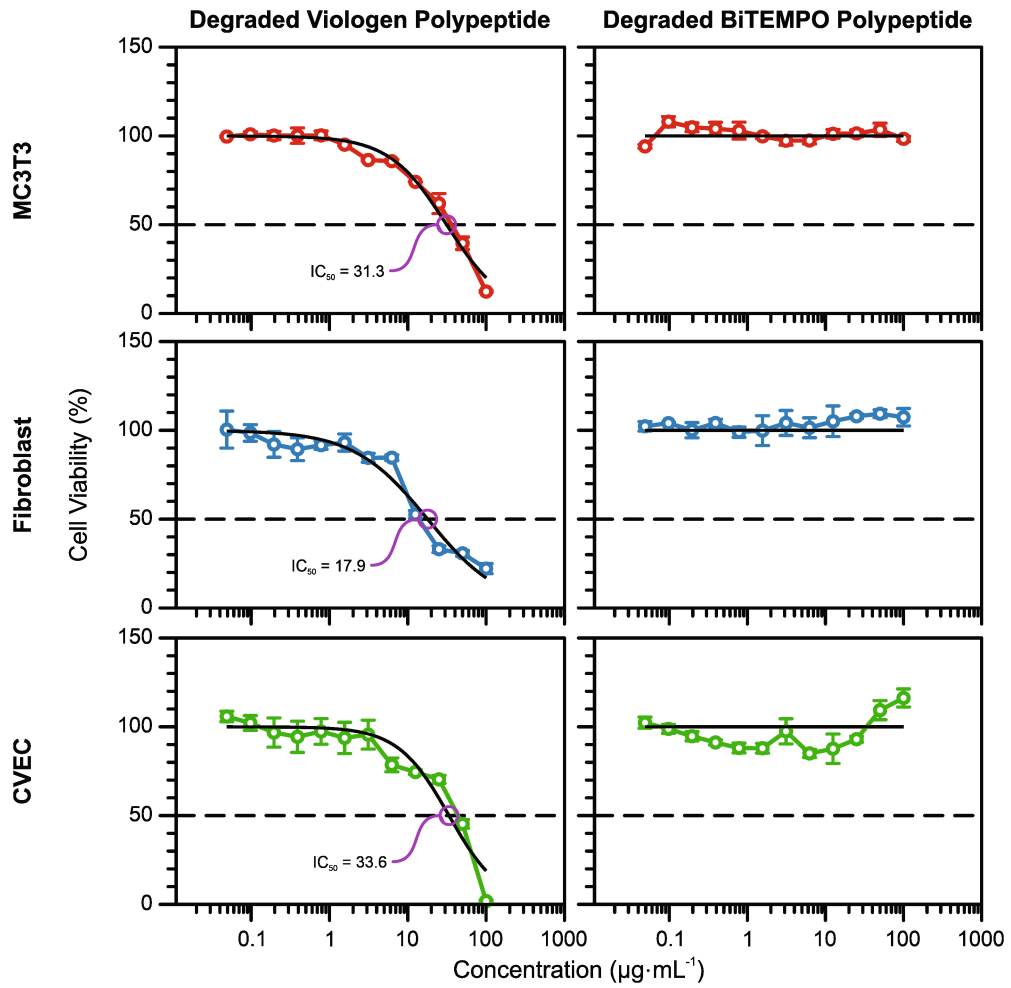


Extended Data Fig. 4 | Electrode morphology before and after testing the full cell. a, b, Scanning electron micrographs of the viol-Cl polypeptide composite electrode (**a**) and the biTEMPO polypeptide composite electrode (**b**),

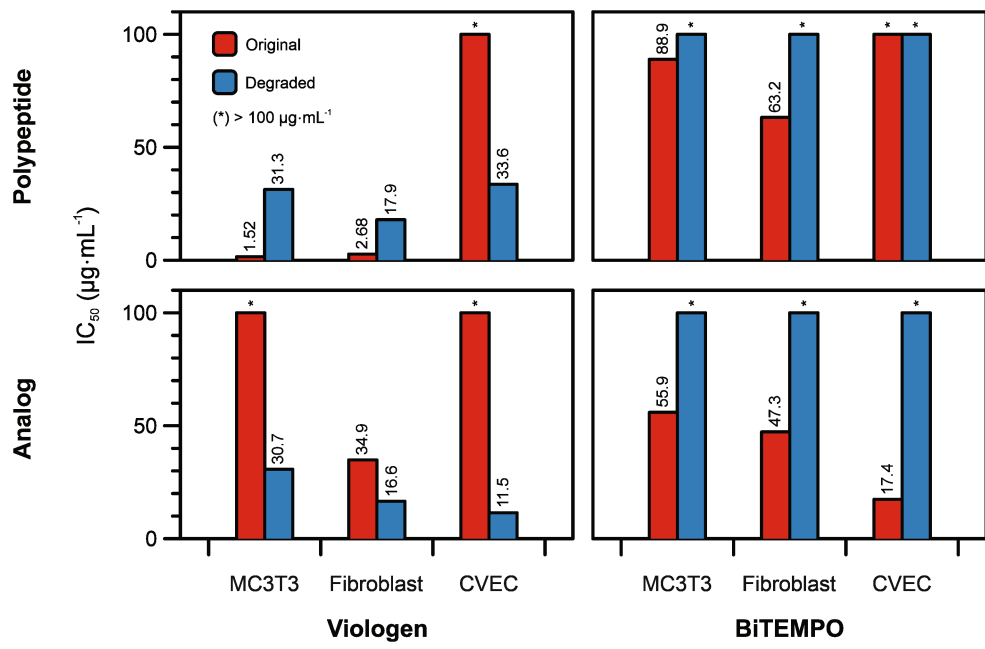
before (i) and after (ii) 50 charge–discharge cycles in the full sandwich cell configuration (viol-Cl polypeptide composite electrode, 0.5 M TBACF₃SO₃ in PC and filter paper, biTEMPO polypeptide composite electrode).



Extended Data Fig. 5 | Cell viability study. Dose–response curves for redox-active polypeptides. Data are expressed as mean \pm s.d. of three determinations. The statistical analysis was performed using GraphPad Prism, with the black lines representing four-parameter fits.



Extended Data Fig. 6 | Cell viability study. Dose–response curves for redox-active polypeptides after acid degradation. Data are expressed as mean \pm s.d. of three determinations. The statistical analysis was performed using GraphPad Prism, with the black lines representing four-parameter fits.



Extended Data Fig. 7 | Cell viability study. Comparison of IC_{50} values of viologen polypeptide, biTEMPO polypeptide, viologen analogue, biTEMPO analogue and their degraded products.

Extended Data Table 1 | Performance of selected polymer-based batteries

Anode	Cathode	Output Potential (V)	C_{spec} (mA·h·g ⁻¹) [*]	E_{spec} (mW·h·g ⁻¹)	Degradable	Ref.
Poly(vinylidibenzothiophenesulfone)	Poly(TEMPO methacrylate)	2.6	~200 [†]	541	No	23
Viologen-chloride Polypeptide	BiTEMPO Polypeptide	1.1 and 1.6	38	60 [‡]	Yes	This Work
Polyviologen hydrogel	Poly(TEMPO acrylamide)	1.1 and 1.5	165	248 [‡]	No	20
Poly(2-methacrylamide-TCAQ)	Poly(2-vinylthianthrene)	1.3	105	137 [‡]	No	5
Poly(anthraquinone-substituted ethyleneimine)	Poly(TEMPO acrylamide)	1.1	80	88 [‡]	No	28
Poly(viologen dibromide)	Poly(TEMPO acrylamide)	1.2	~100 [†]	120	No	7
Hydroquinonesulfonic acid potassium salt [§]	<i>p</i> -Benzoquinone [§]	0.8	~42 [†]	32	Yes	8
Poly(galvinoxylstyrene)	Poly(TEMPO-substituted norbornene)	0.7	32	22 [‡]	No	21
Poly(nitronylnitroxylstyrene)	Poly(galvinoxylstyrene)	0.6	29	17 [‡]	No	22

Data from this work and refs. ^{5,7,8,20-23,26}. TCAQ, 11,11,12,12-tetracyano-9,10-anthraquinonedimethane; C_{spec} , specific capacity; E_{spec} , specific energy.

^{*}Value taken from the first charge–discharge cycle.

[†]Value estimated from the charge–discharge graph in the relevant reference.

[‡]Value calculated by multiplying specific capacity by output voltage (largest voltage if two are listed).

[§]Small-molecule organic redox-flow battery.

Extended Data Table 2 | Elemental analysis of the synthesized polymers

Polymer		% C	% H	% N	% Cl
PCHLG ₅₀	Calc'd	53.49	7.38	5.70	NA
	Found	53.63 (0.14)*	7.43 (0.05)	5.62 (0.08)	NA
PIHLG ₅₀	Calc'd	39.45	5.44	4.20	NA
	Found	39.66 (0.21)	5.57 (0.13)	4.31 (0.11)	NA
Viologen-iodide Polypeptide	Calc'd	41.62	4.63	6.60	NA
	Found	41.35 (0.27)	4.91 (0.23)	6.35 (0.25)	NA
Viologen-chloride Polypeptide**	Calc'd (w/o H ₂ O)	58.21	6.48	9.23	15.47
	Calc'd (w/ 140 H ₂ O)	52.46	6.95	8.32	13.95
	Found	52.36 (0.10)	6.97 (0.02)	8.04 (0.28)	14.10 (0.15)
PPLG ₅₀	Calc'd	57.64	5.54	8.40	NA
	Found	57.50 (0.14)	5.50 (0.04)	8.51 (0.11)	NA
PPLG ₅₀ -g-MTEMPO	Calc'd	56.88	8.28	5.85	NA
	Found	56.65 (0.23)	8.31 (0.03)	5.97 (0.12)	NA
BiTEMPO Polypeptide	Calc'd (for 18% oxoammonium cation)	51.40	6.82	5.21	NA
	Found	51.57 (0.17)	7.20 (0.38)	5.57 (0.36)	NA

NA, not applicable.

*The numbers in parentheses reflect the differences between calculated and observed values.

**The viol-Cl polypeptide is hygroscopic. Under vacuum, the polymer is dark brown; upon exposure to air it quickly turns yellow.

Article

Extended Data Table 3 | Degradation conditions used for the viologen and biTEMPO polypeptides

[HCl] \ T	r.t.	50 °C	80 °C	110 °C
0.01 M	No degradation	No degradation	No degradation	No degradation
1 M	No degradation	Partial degradation (side chains)	Partial degradation (side chains)	Complete degradation
6 M	No degradation	Partial degradation (side chains)	Partial degradation (side chains)	Complete degradation